International Journal of Nanoelectronics and Materials
Volume 14, No. 4, October 2021 [357-372]

Solutions-Processed Cu_2ZnSnS_4 Solar Cell utilizing Zn Powder as Local Material

Eka Cahya Prima[1*], Angela Vitadewi[2], Anggi Datiatur Rahmat[2], Endi Suhendi[2], Suyatman[3], Brian Yuliarto[3]

[1]*Solar Energy Materials Laboratory, Department of Science Education, Faculty of Mathematics and Science Education, Universitas Pendidikan Indonesia, Bandung 40154, Indonesia*
[2]*Materials Science Laboratory, Departement of Physics Education, Faculty of Mathematics and Science Education, Universitas Pendidikan Indonesia, Bandung 40154, Indonesia.*
[3]*Advanced Functional Materials Laboratory, Department of Engineering Physics, Faculty of Industrial Technology, Institut Teknologi Bandung, Bandung 40132, Indonesia*

Received 13 December 2020, Revised 17 March 2021, Accepted 6 May 2021

ABSTRACT

Indonesia, as any other countries, requires high electrical energy consumption. The primary electrical supply in Indonesia is dominated by the limited and high pollution fossil fuel. Solar energy is needed as alternative renewable energy to overcome the limited fossil fuels. The Cu_2ZnSnS_4 (CZTS) as an absorber is a good material due to its non-toxic property, environmentally friendly, low cost and elemental abundance. CZTS solar cells have a high theoretical efficiency of up to 30.9%. The abundance of mineral resources in Indonesia (especially 99% Zinc powder) is utilized for the first time to replace the standard material from Zinc Acetate Dihydrate. Cu-poor Zn-rich CZTS/CdS/ITO is made using Zinc local material compared to the Zinc Acetate Dihydrate. The fabrication technique is carried out using a solution-processed method and spin-coating deposition. The Zn to Sn ratio is investigated towards the crystallinity, morphology, optical properties and cell performance. The result shows that Zinc local material in the CZTS absorber increases the percentage of kesterite phase by 0.3 % compared to Zinc acetate (standard material) and increases the crystallite size by 38.26 nm. The best cell has an efficiency of 5.10 ×10^{-4} % for Z125 sample (Zn/Sn ratio of 1.25) due to better crystallinity, morphology, optical properties.

Keyword: Cu_2ZnSnS_4 Thin Film, Sol-Gel Method, Solution Process, Kesterite, Solar Cells

1. INTRODUCTION

In 2018, Indonesia's electrical energy consumption was 281,976.21 GWh, increasing by 5% per year [1]. The primary electrical energy supply in Indonesia is dominated mainly by fossil fuel, especially coal (50%), gas (29%), oil (7%) while it contains merely 14% renewable energy sources. Solar plant power contributes only 0.09% of total electrical energy consumption [2-4]. It can be seen that fossil fuel power plants are still very dominant and are one of the causes of oil and natural gas supply depletion and high pollution due to greenhouse gas emissions such as carbon dioxide, triggering extreme climate change and global warming [5, 6]. It is estimated that in the next 23 years, the world oil supply will run out and in the next 62 years, the natural gas

* Corresponding author: ekacahyaprima@upi.edu

supply will also run out. Meanwhile, in Indonesia, oil and gas supplies are expected to run out in the next 18 years. Renewable energy is needed to be an alternative to the limited fossil fuels that are not environmentally friendly [7, 8].

Solar radiates enormous energy. Considering Indonesia is a tropical country located on the equator, Indonesia has a significant potential of solar energy up to 500 GW or seven times larger than the total installed electricity capacity [9-12]. The conversion of solar energy to electricity plays an essential role in overcoming Indonesia's dependence on fossil fuels. Solar cells convert solar energy into electrical energy by utilizing photovoltaic materials' electrical properties, namely semiconductors [13]. Solar cells are made of p-type and n-type semiconductor materials connected so that the diffusion of charge carriers occurs and a depletion area is formed [13, 14]. There are four stages of energy conversion by photovoltaic: 1) Absorption, 2) Separation, 3) Collection and 4) Recombination. The solar cell absorber absorbs about 45% sunlight spectrum with a bandgap of 1.1 - 1.4 eV [15-26].

The high cost of manufacturing solar cells is why photovoltaics are only used for 0.09% of Indonesia's total electrical energy consumption and 1% of world energy consumption, although it has many advantages. Therefore, the cost of producing solar cells needs to be reduced significantly to produce cheap solar cells with a good performance so that they can compete in the market to enter the multi-terawatt era (TW). Generally, 50% of the cost of making solar cells relates to other component and installation requirements such as inverters, wiring and structural installation costs. Thus, the key to reducing solar cells' cost is the efficiency of a solar cell, the main element's price and the fabrication. The higher efficiency can reduce photovoltaic costs because more energy is produced in the solar cell's lifetime. Goodrich et al. stated that the cost per watt (Wp) decreases as efficiency increases. This trend is due to the cost of power such as module and inverter components, which increase capital costs as efficiency increases. However, it was found that the cost per Wp began to remain constant when the solar cell had an efficiency above 15% [27-29]. Therefore, solar cells' commercial efficiency is targeted to be at least 15% or lab efficiency of 20% to significantly reduce the cost of making photovoltaics.

Solar cells commercially produced today are silicon-based solar cells. This semiconductor has an indirect bandgap so that the absorption coefficient tends to be lower compared to a semiconductor with a direct bandgap. Therefore, the photovoltaic type with direct bandgap is used as an alternative to replace indirect bandgap semiconductors [30]. This semiconductor is called the light absorption layer (absorber). Absorber that has high efficiency includes GaAs, CdTe and CIGS [31, 32]. This material's performance can be used as commercial solar cells, but they have their drawbacks. GaAs and CdTe consist of toxic substances of Arsenic and Cadmium and these limit their commercial use. As for CIGS, the use of Indium reduces its potential to reach a terawatt scale because of its high price and limited supplies of materials for an industrial scale.

CZTS as an absorber can overcome this limitation due to its non-toxic property, environmentally friendly, low cost and elemental abundance. CZTS also have high SQL up to 30.9% (for 1.0 eV bandgap). CZTS raw materials production can supply electricity on a terawatt scale [13, 28, 33-35]. CZTS consists of elemental abundance, namely Cu, Zn, Sn and S. Total of Indonesia's mineral resources in 2019 for these elements are; 16.355 million tons of Copper ore with reserves of 1.8 million tons; 12.82 million tons of Zinc ore with reserves of 32.5 million tons; 11.9 million tons of Tin ore with reserves of 1308.9 million tons; 1.7 million tons of Sulfur ore with reserves of 2.6 million tons [2, 36, 37]. The abundance of mineral resources in Indonesia (especially Zinc) is the motivational background for this research. Since local Zinc prices are cheaper than imported materials, it brings hope that local materials can be utilized for renewable energy sources. The Indonesia energy regulation stated that by 2025, Indonesia would utilize 5% of energy resources from renewable energy. The installed photovoltaic is still 200 MW, whereas the country still harvests 0.08% of solar energy corresponding to the tropical region's real solar energy potential. In the Indonesian marketplace, 12 industries have still focused on producing silicon-based solar

cells. The work will supply low-cost, abundant material for future industrial third-generation solar cells in Indonesia by considering this research.

The CZTS-based thin-film solar cell has the highest efficiency of 12.6 % fabricated through solution-process-based fabrication with CZTS deposition using a spin-coater [38]. Various phenomena in the CZTS bulk and its interface, such as recombination and secondary phase, cause CZTS solar cells' practical efficiency to be lower than CIGS-based solar cells' efficiency [17, 39, 40]. CZTS is formed in large numbers in the secondary phase because the thermodynamic stability of the secondary phase of CZTS is more stable than the CZTS kesterite phase's stability [41]. This condition can be overcome using a Cu-poor Zn-rich composition so that the destructive Cu_2SnS_3 secondary phase will be reduced, and a better ZnS secondary phase will be formed in larger quantities [42]. The secondary phase of ZnS can still reduce solar cells' performance by forming traps that slow down the transport of charge carriers, although the impact is not as bad as the Cu_2SnS_3 secondary phase.

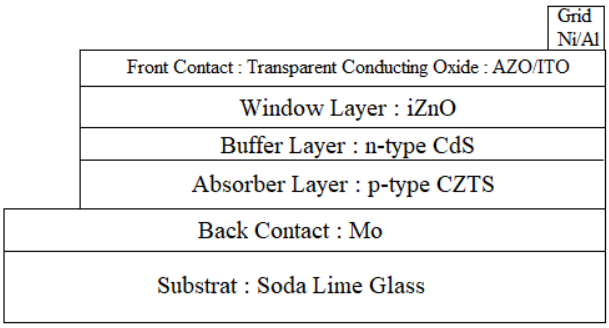

Figure 1. The primary device structure of CZTS based thin-film solar cells

Figure 1 shows the basic device structure of CZTS based thin-film solar cells [34]. This structure was adopted from the CIGS device structure because of their structural similarity [31, 32]. A Mo film layer with a thickness of 0.5–1.0 μm was positioned on the SLG substrate as a back contact. This Mo layer serves as an ohmic contact for CZTS. The film precursor or CZTS film nanoparticles are first formed and positioned on the back contact Mo. This process is followed by annealing in an inert or reactive atmosphere to initiate the CZTS nucleation and growth. Thus, a CZTS absorber p-type layer between 0.6-2.0μm thick was formed above Mo. This layer serves to absorb light (absorber). The n-type buffer layer is then made to form a p-n junction with a p-CZTS type absorber. Most CZTS-based solar cells use n-CdS with a thickness of 50 nm, usually through the fabrication method of heterojunction chemical bath deposition. The device structure is equipped with a 50-100 nm high resistive buffer layer as a window layer like i-ZnO with the sputtering method.

In this study, Cu-poor Zn-rich CZTS/CdS/ITO solar cell was synthesized by the solution-processed method. The research will be conducted on five samples made with Zinc powder, Copper Acetate Monohydrate, Tin Chloride and Thiourea with different Zn/Sn ratios and fixed Cu/(Zn + Sn) ratios. Samples were made with CZTS standard precursor material, namely Zinc Acetate Dihydrate, Copper Acetate Monohydrate, Tin Chloride and Thiourea comparison. Zinc is investigated due to a higher absorption coefficient, larger particle size and lower purity, which is predicted to reduce the bandgap and increase the absorption spectrum, that will improve solar cell performance or replace standard materials to reduce production costs. However, Zinc is more difficult to dissolve (less soluble) because of its relatively large size. This issue can be settled by using a solution-processed fabrication technique followed by a sulfurization process to grow grain and binding atoms that are difficult to bond. The spin coating method was used to deposit the precursor. The crystals' composition and size were analyzed by XRD, the morphology of the CZTS absorber thin layer was analyzed using SEM, the optical and bandgap properties were

analyzed using UV-Visual spectroscopy, while the performance was tested through the characteristics of the J-V curve. The results are expected to increase the efficiency of CZTS-based thin-film solar cells.

2. RESEARCH METHOD

CZTS Thin Film Preparation: CZTS thin films were prepared by solution-processed. Figure 2 shows the device structure of all six samples used. Five samples were made using Zinc powder (Z) as a local material and one sample was made using 0.52 M Zinc Acetate (ZA) as a standard material. Each sample has constant ratio of Cu/(Zn+Sn) = 0.86 and different ratio of Zn/Sn = 1.15, 1.20, 1.25, 1.30, 1.35. The precursor was made by dissolving Copper Acetate Monohydrate, Zinc Acetate Dihydrates (ZA) or Zinc Powder (Z), Tin Chloride and 2.06 M Thiourea with the specific components as shown in Table 1 with 2-methoxy ethanol as the solvent.

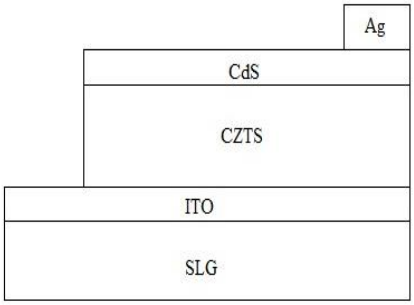

Figure 2. Device structure of all 6 samples

TABLE 1. Composition of precursor

Sample	Zn/Sn	Zinc Acetate Dihydrate(N)/Zinc Powder(L) (mol/L)	Tin Chloride (mol/L)
ZA125	1.25	0.34	0.27
Z115	1.15	0.32	0.28
Z120	1.20	0.33	0.27
Z125	1.25	0.34	0.27
Z130	1.30	0.34	0.26
Z135	1.35	0.35	0.26

The precursor was dissolved at 500 °C for 2 hours using a magnetic stirrer. After 1 hour of dissolving, few drops of TMA and MEA were added to the solution as a stabilizer. Before spin-coating deposition, the 2 × 2 cm SLG/ITO glass substrate was washed with isopropyl and DI water 1:1 with an ultrasonic cleaner and dry with a hot blower to remove unwanted particles on the surface of the substrate. The solution was spin-coated at 3000 rpm for the 30 s, annealed in air at 200 °C for 2 min to remove residuals organic materials and cooled down for 5 min. The "spin coating-annealing" process was repeated 14 times to obtain 1 μm thickness of the CZTS absorber layer. The substrate was then sulfurized in the air at 550 °C for 30 minutes. The sulfurization was started by placing the deposited film sealed in a stainless steel tube and sulfur powder to reduce sulfur loss and annealed it in the furnace. Figure 3 shows the six samples before and after sulfurization.

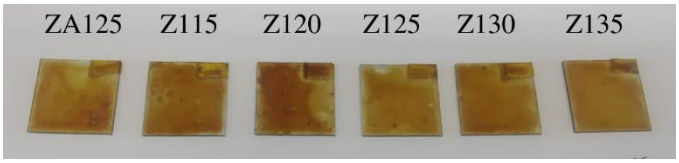

(a)

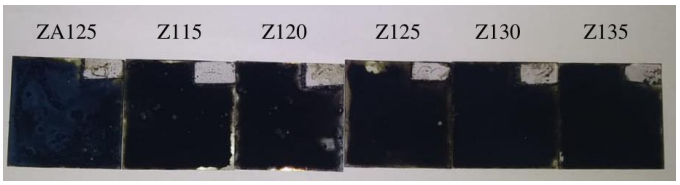

(b)

Figure 3. The six samples: (a) before sulfurization (b) after sulfurization

Device Fabrication: Cadmium sulfide was deposited on the SLG/ITO/CZTS substrate by Chemical Bath Deposition (CBD). The bath was prepared by dissolving 20 mL 0.75 M Thiourea, 20 mL 0.015 M $CdSO_4$ and 22 mL 25 % NH_4OH in 140 mL DI water. The CBD was performed at 80 ^oC for 9 min to obtain ~50 nm CdS and the bath was continuously stirred during the process. The SLG/ITO/CZTS/CdS substrates were then washed with DI water using an ultrasonic cleaner. All samples were subjected to post-annealing treatment at 250 ^oC for 15 min. The silver paste was used as a current collector, place in the corner of the substrate and dried at 50 ^oC.

Characterization: The samples were characterized using XRD to determine the CZTS absorber layer's crystal phase. The XRD data of thin films were characterized using Bruker D8 Advance. The samples' characterization results were then compared and matched with the diffraction patterns of both the kesterite phase and its secondary phase that might emerge, based on references taken from the Crystallography Open Database (COD). SEM characterization was carried out to observe the CZTS absorber thin layer's surface morphology, namely the uniformity of particle size on the CZTS absorber thin layer's surface. Electrical properties were examined using Current-Voltage characteristics measured by ADCMT 6242 Multimeter and optical properties were characterized using V1600PC 190-1100 nm Ultraviolet-Visible Spectrophotometer. The absorbance data will be used to obtain bandgap, Urbach energy, and light-harvesting efficiency (LHE). The bandgap was obtained using Tauc's Plot method with equation (1):

$$(\alpha hv)^{\frac{1}{r}} = k(hv - E_g) \quad (1)$$

where: r = ½ for *allowed direct transition;* r = 3/2 for *forbidden direct transition;* r = 2 for *allowed indirect transition* and r = 3 for *forbidden indirect transition.* The LHE was obtained using the equation (2):

$$LHE\ (\%) = (1 - 10^{-\alpha}) \times 100\% \quad (2)$$

3. RESULTS AND DISCUSSION

3.1 Structural properties

The samples were characterized using XRD to determine the crystal phase formed in the CZTS absorber layer. The samples' characterization results were then compared and matched with the diffraction patterns of both the kesterite phase and its secondary phase that might emerge, based on references taken from the Crystallography Open Database (COD).

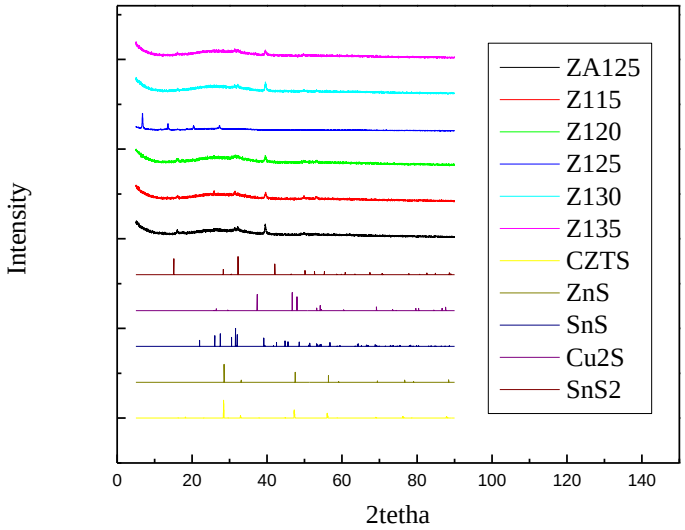

Figure 4. XRD diffraction pattern shows the formation of ZnS, SnS, Cu_2S and SnS_2 as secondary phases

Figure 4 shows that the samples have a diffraction pattern with a high noise level than the reference pattern. This result shows that the material is amorphous. When compared, Z125 has the lowest noise diffraction pattern, indicating that this sample has the highest crystallinity. However, the samples did not show any predominant kesterite peaks. This result means that the percentage of the kesterite phase in the samples is deficient. The sulfurization process carried out in the air atmosphere using stainless steel is failed and resulted in a low crystallinity (amorphous) level and the kesterite phase was difficult to form. Sulfurization must be done in Argon, Nitrogen, or even vacuum atmospheres to reduce sulfur loss due to the reaction between oxygen and sulfur. This research also analyzes the tendency of secondary phases resulted during the synthesis of CZTS.

TABLE 2. The effect of Zinc concentration towards CZTS kesterite formation and its secondary phases analysis from XRD diffraction patterns using Match

Sample	Mass percentage (%)					
	Cu_2ZnSnS_4	Cu_2SnS_3	ZnS	Cu_2S	SnS	SnS_2
ZA125	7,9	15,8	8,9	44,2	13,8	9,4
Z115	7,0	9,7	1,4	74,7	5,8	1,4
Z120	0,6	6,4	1,5	74,7	15,6	1,3
Z125	8,2	16,3	9,2	42,3	14,3	9,7
Z130	8,2	16,3	9,2	42,3	14,3	9,7
Z135	5,6	11,2	6,3	60,3	9,8	6,7

Table 2 shows the mass percentage of the crystal phase formed in the samples. It can be seen that the Z125 sample has the highest mass percentage of the kesterite phase compared to other samples. For the same ratio, Zinc material's use increases the kesterite phase percentage by 0.3% compared to Zinc Acetate.

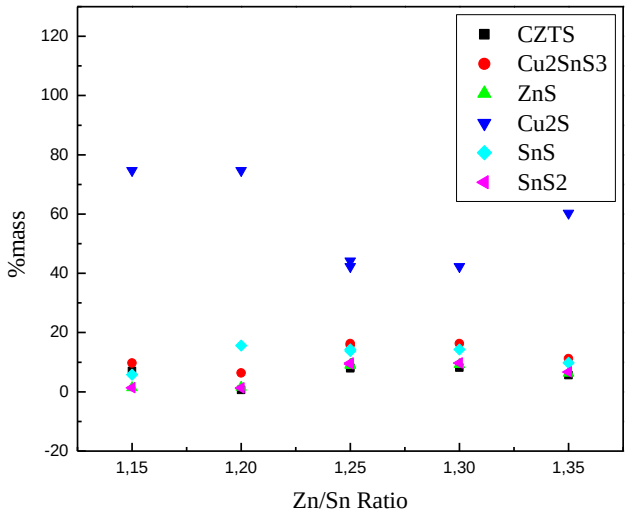

Figure 5. The effect of the Zn/Sn ratio on the crystalline phase formed in the samples

Figure 5 shows that the crystal phase that dominates the six samples is the Cu_2S phase. Z115 and Z120 have the highest mass percentage of Cu_2S, which is almost ½ - ¾ of their total mass. For the same Zn/Sn ratio, Zinc has reduced the secondary phase percentage of Cu_2S by 1.9% compared to Zinc Acetate. Z125 also has the smallest percentage of secondary phase Cu_2S compared to other samples. The dominance of the Cu_2S phase indicates that the Copper Acetate is not evenly mixed in the precursor and is the cause of the resulting blue color on the precursor. This phenomenon also supports the absorbance spectrum results where the absorbance spectrum of the absorber does not appear to absorb the blue wavelength (400-500 nm) at all. Cu tends to bind sulfur alone and form Cu_2S when sulfurized. It indicates that it is necessary to stir the Copper Acetate longer or at a higher temperature so that the Copper Acetate is better dissolved in the solvent.

TABLE 3. The average crystallite size of the CZTS absorber from each sample

Sample	Crystallite Size (nm)
ZA125	58,87
Z115	20,15
Z120	17,52
Z125	97,13
Z130	45,80
Z135	44,24

Apart from the crystal phase, XRD data was also used to determine the six samples' crystallite size using the Scherrer Equation. As seen in Table 3, the Z125 sample has the largest mean crystallite size than the other samples, whereas samples Z115 and Z120 have sample sizes that are not much different, so do samples Z130 and Z135.

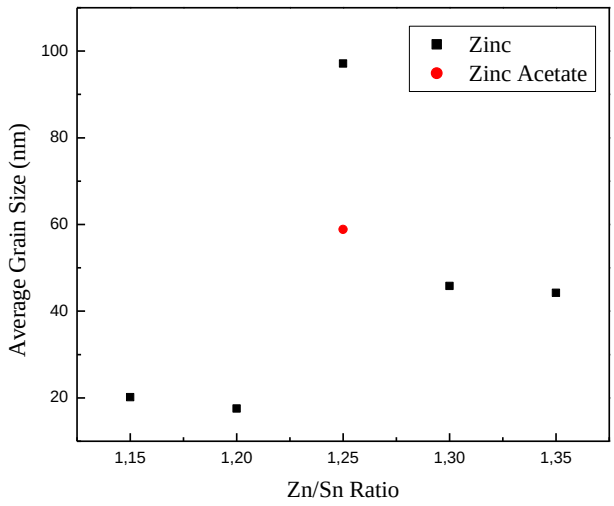

Figure 6. The effect of Zn/Sn ratio on crystallite size

Figure 6 shows that Zinc material use results in a much larger crystallite size than Zinc Acetate for the same ratio. The result is consistent with the initial study's prediction that Zinc material can increase the crystallite size of the CZTS absorber. Crystallite size will affect solar cells' performance because it can increase the absorption coefficient and decrease the bandgap, resulting in better efficiency.

3.2 Morphological properties

SEM characterization was carried out to observe the CZTS absorber thin layer's surface morphology, namely the uniformity of particle size on the CZTS absorber thin layer's surface.

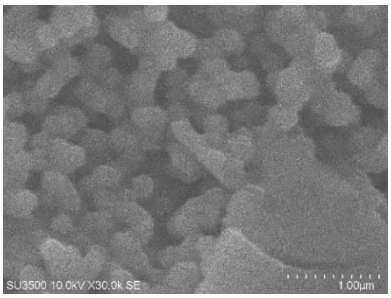

(a) ZA125

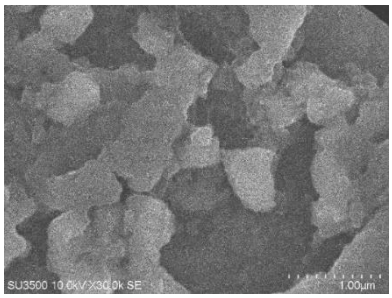

(b) Z115

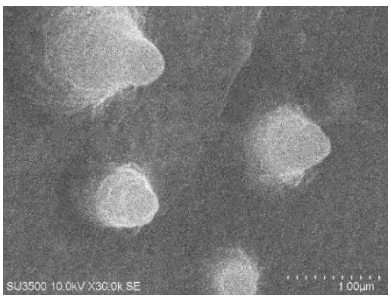

(c) Z120

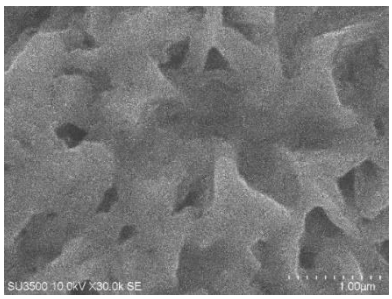

(d) Z125

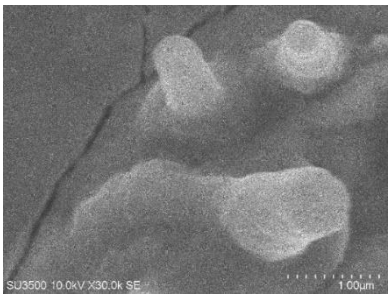

(e) Z130

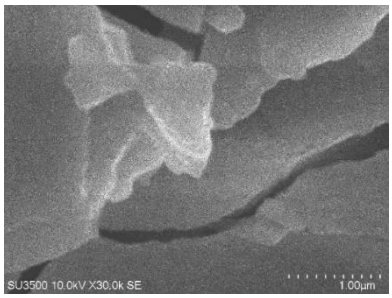

(f) Z135

Figure 7. Surface morphology of CZTS absorber layer

Figure 7 shows the surface morphology of the CZTS absorber film for the six samples. It can be seen that the sample with a Zn/Sn ratio of 1.25 produces a high level of size uniformity using both Zinc and Zinc Acetate materials. There are similarities in particle size between Z115-Z120, Z125 - ZA125 and Z130-Z135. The result supports the results regarding crystallite size based on XRD. Furthermore, samples with a Zn/Sn ratio of more than 1.25 cracked on their surface. The greater the Zn/Sn ratio, the more destructive the surface of the sample. The addition of excessive Zinc can damage the surface of the thin film. Samples using Zinc material produce the best morphology seen in sample Z125.

3.3 Optical properties

The first optical properties based on absorbance are observed from the six CZTS-based solar cells. Absorbance or optical density indicates the amount of light absorbed by a material at a particular wavelength. Figure 8 shows that the six samples have an absorbance spectrum with a pattern that tends to be the same, with two peaks at a wavelength around 700 nm and 300 nm. The six samples are sensitive at short wavelengths. The use of Zn material does not significantly change the optical properties of the CZTS absorber layer. Z125 owns the highest absorbance peak, with the maximum absorbance of the first peak is 2.211 at a wavelength of 310 nm and the second peak is 0.429 at a wavelength of 665 nm. Consequently, Zn material's use slightly increases the height and width of the absorbance spectrum of the CZTS absorber.

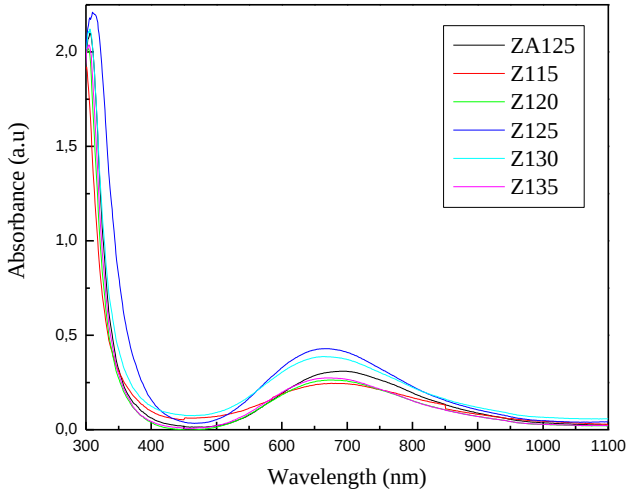

Figure 8. Absorbance Spectrum of CZTS Absorber

Overall, the six samples produced a similar absorbance spectrum pattern, namely the existence of a valley in the 400-500 nm wavelength range. It indicates that the sample does not absorb the wavelength of blue light at all. Furthermore, the precursor is blue in color because the material as a whole emits blue light. Compared with the resulting phase, this blue color is a characteristic of the Copper Acetate material because the Copper Acetate does not mix properly and causes the precursor to turning blue. Thus, when it is sulfurized, Copper Acetate tends to bind sulfur alone

and form a Cu_2S phase which is more dominant than kesterite. In addition to the absorbance spectrum, the optical property that will be reviewed is Light Harvesting Efficiency (LHE). LHE is analyzed to determine the percentage of light absorbed in a specific wavelength range.

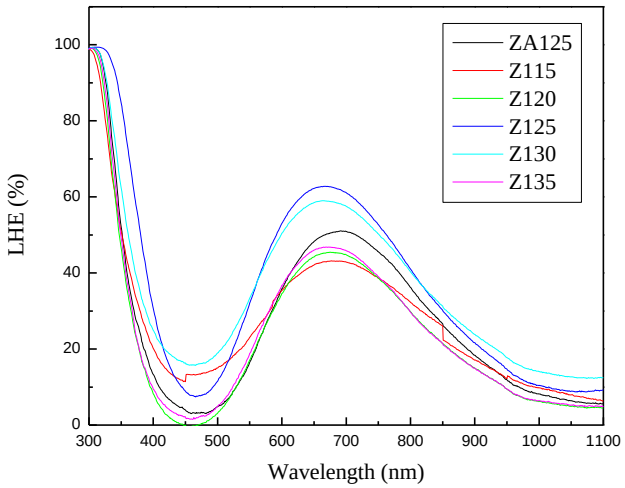

Figure 9. Light-Harvesting Efficiency of CZTS absorber

Figure 9 show that the six samples have a similar LHE spectrum pattern. That is, all of them have two peaks at wavelengths of around 700 nm and 300 nm. The samples are sensitive at short wavelengths. The use of Zn material does not significantly change the optical properties of the CZTS absorber layer. The highest LHE peak is owned by Z125, with the maximum LHE percentage of the first peak is 99.38 % at a wavelength of 310 nm and the second peak is 62.78 % at a wavelength of 665 nm. Consequently, the use of Zn material slightly increases the percentage of LHE. UV-Vis Spectroscopic data can be analyzed to determine the bandgap of a material using the Tauc's Plot method. Figure 10 shows the Tauc curve for determining the bandgap of the six samples.

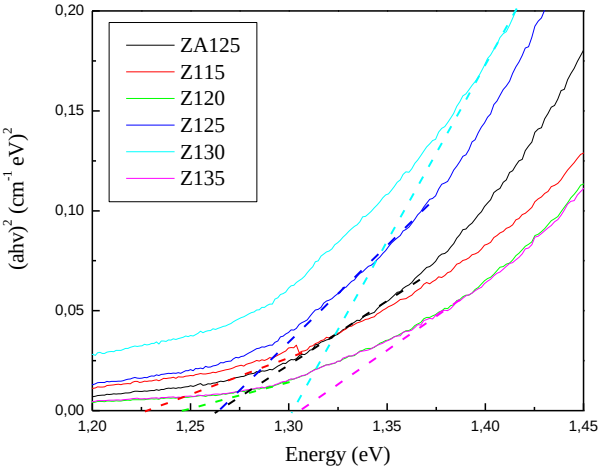

Figure 10. Determination of energy gap by extrapolation method from the variation of $(\alpha h\nu)^2$ vs. $h\nu$ for each sample

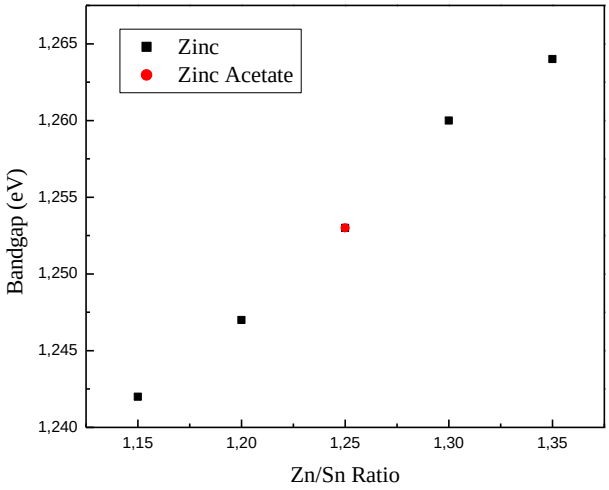

Figure 11. The effect of Zn/Sn ratio on the bandgap

If the bandgap of the six samples is plotted against the Zn/Sn ratio as in Figure 11, it can be seen that the curve shows a linear relationship, where the greater the Zn/Sn ratio, the higher the bandgap. For the same Zn/Sn ratio, both Zinc and Zinc Acetate materials produce the same bandgap size, namely 1.253eV.

TABLE 4. The IPCE analysis for the Cu_2ZnSnS_4 thin-film solar cells

Sample	First Peak			Second Peak			Bandgap (eV)
	λ_{max1} (nm)	Absorbance (a.u)	LHE (%)	λ_{max2} (nm)	Absorbance (a.u)	LHE (%)	
ZA125	306	2.100	99.20	693	0.310	51.05	1.253
Z115	301	1.920	98.79	677	0.245	43.19	1.242
Z120	304	2.017	99.03	675	0.263	45.45	1.247
Z125	310	2.211	99.38	665	0.429	62.78	1.253
Z130	306	2.121	99.24	666	0.387	58.98	1.260
Z135	305	2.036	99.08	665	0.274	46.82	1.264

Table 4 shows all the six samples' optical properties, including the optimal wavelength, absorbance efficiency, LHE and bandgap. It appears that the use of the Zn material does not significantly change the optical properties of CZTS. When compared, for the same ratio, ZA125 and Z125 have the same bandgap value. Moreover, the Zn material can be used as an absorber without changing its optical properties significantly. The use of Zn material slightly increased the absorbance spectrum and LHE and did not change its bandgap. Z125 owns the highest absorbance and LHE values.

3.4 Device performance

The performance tested in this study is the electrical performance of solar cells. The performance of solar cells is generally represented in terms of efficiency. Efficiency is defined as the ratio of the energy output produced by solar cells to solar energy input. In addition to efficiency, J_{sc}, V_{oc}, and Fill Factor are also calculated to represent a CZTS-based solar cell device's performance.

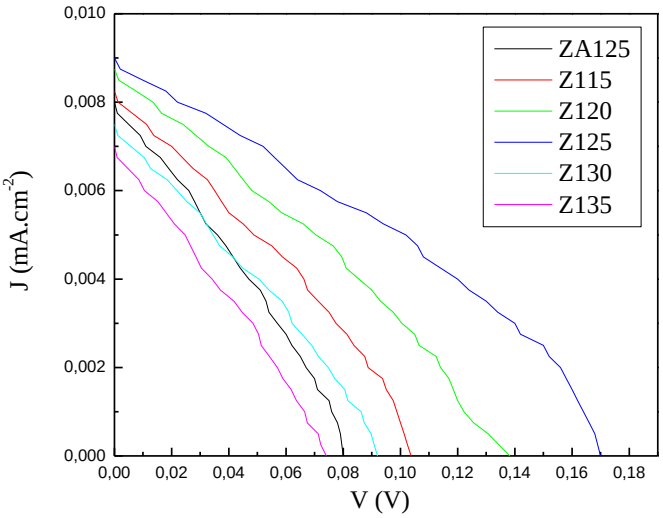

Figure 12. Photovoltaic performance of CZTS based solar cell

Figure 12 shows the J-V characteristic curves for the six samples. The graph shows that Z125 has the highest V_{oc} and J_{sc}, and Z135 has the lowest V_{oc} and J_{sc} because the surface of the Z135 cracks and causes a decrease in the V_{oc} value and an increase in the material's internal resistance so that the resulting current density is also small.

Table 5. Photovoltaic performance for the Cu_2ZnSnS_4 thin-film solar cells

Sampel	Zn/Sn Ratio	Bandgap (eV)	V_{oc} ($\times 10^{-1}$ V)	J_{sc} ($\times 10^{-3}$ mA.cm^{-2})	FF (%)	η ($\times 10^{-4}$%)
ZA125	1.25	1.253	0.080	8.00	29.8	1.91
Z115	1.15	1.242	0.104	8.25	31.6	2.71
Z120	1.20	1.247	0.138	8.75	30.0	3.63
Z125	1.25	1.253	0.170	9.00	33.3	5.10
Z130	1.30	1.260	0.092	7.50	29.7	2.05
Z135	1.35	1.264	0.074	7.00	28.2	1.46

Table 5 shows that Z125 has the highest efficiency than other samples and Z135 gives the lowest efficiency. For the same ratio, Zinc's use can improve CZTS-based solar cells' performance compared to using Zinc Acetate material.

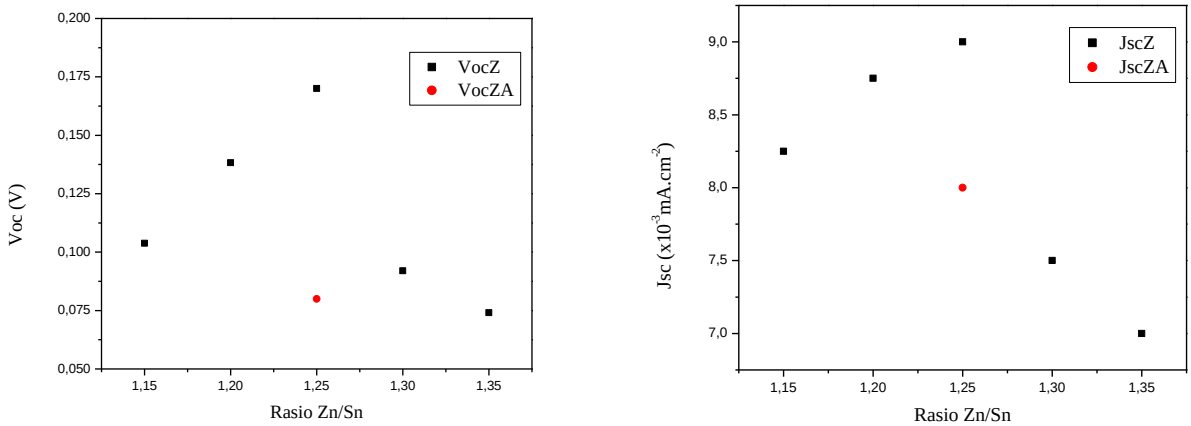

(a) (b)

Figure 13. The effect of Zn/Sn ratio on (a) V_{oc} and (b) J_{sc}

Figure 13 shows that the Z125 sample produces the highest V_{oc} and J_{sc}. When the material ratio is 1.15-1.25, the resulting V_{oc} and J_{sc} tend to increase. However, when the Zn/Sn ratio was increased more than 1.25 V_{oc}, J_{sc} decreased drastically due to the use of too much Zinc, which is destructive to the thin layer surface, makes cracks and forms traps hence the resulting current decreased drastically.

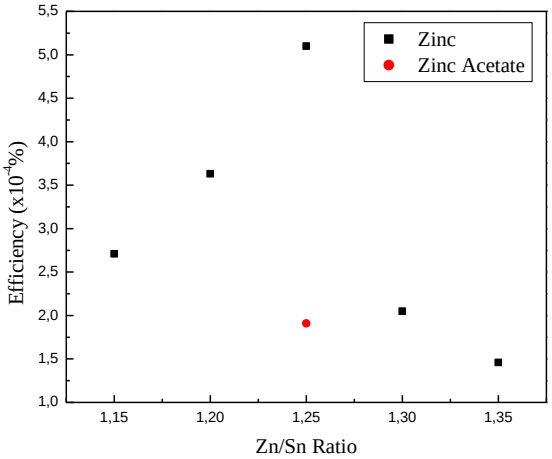

Figure 14. The effect of Zn/Sn ratio on efficiency

Figure 14 shows the effect of the Zn/Sn ratio on the efficiency of CZTS-based solar cells. It can be seen that the Zn/Sn ratio between 1.15-1.25 results in better efficiency compared to other samples, where the Zn/Sn ratio produces the highest efficiency. This evidence is following the results of previous studies, which state that the optimal ratio of Zn/Sn for CZTS is in the range between 1.1-1.25 [15, 16, 34]. For the same ratio, the use of Zinc (Z125) compared to Zinc Acetate (ZA125) also improves the performance of solar cells in the form of increased efficiency, V_{oc} and J_{sc}. The result is supported by XRD results where the Z125 sample had the highest kesterite phase, the largest crystallite size, the morphology with the most uniform particle size (uniform), the absorbance size and high LHE and the optimized bandgap. It means that the optimal Zn/Sn ratio is 1.25 and the use of Zinc in replacing Zinc Acetate can improve performance by increasing crystallite size so that the absorption coefficient increases, thereby increasing V_{oc} and J_{sc} [34]. However, Zinc's excessive use can damage the CZTS absorber thin layer's surface, increase the secondary phase, reduce the morphological quality by forming cracks and size unevenness and reduce optical properties and performance [43]. Therefore, the right Zn/Sn ratio in making CZTS ranges between 1.15-1.25. More than that, Zinc's presence will be very destructive.

The six samples still have a relatively very small efficiency compared to previous studies' results when analyzed further. This result is affected by several factors such as grain size, grain boundaries of the CZTS absorber layer, differences in thickness and the cell's active surface area [43, 44]. The limitations of the tools during the experiment, such as the absence of a vacuum tube or the standard set of sulfurization tools, also caused the sulfurization process's failure, resulting in low crystallinity (amorphous) materials, making it difficult to obtain better efficiency. The effect of sulfurization is very significant because, in the process, the CZTS begins to bind completely and grow grain and produce structures with high crystallinity [16, 45-47]. So, if the sulfurization is not done optimally, it will significantly impact the solar cells' efficiency. Besides, due to limited tools and materials, the fabricated layer is also fundamental. There is no anti-reflection layer, window coating, or TCO, so that light absorption and electron transfer on the device is not optimal enough [46, 48]. Therefore, there is a loss mechanism so that the material does not optimally absorb light. This mechanism is the reason for the low performance of the solar cells produced in this study.

4. CONCLUSION

The use of Zinc local material in a thin layer of CZTS-based solar cell absorber increases the percentage of kesterite phase by 0.3 % compared to Zinc acetate (standard material) and increases the crystallite size by 38.26 nm. The use of Zinc material does not significantly change the morphology of the CZTS-based solar cell absorber layer. Using both Zinc and Zinc Acetate, the uniformity of size is almost the same. However, using too much Zinc can cause cracks on the surface of the thin absorber layer. The use of Zinc material does not significantly change the CZTS-based solar cell absorber layer's optical properties. The use of Zn material in the CZTS absorber slightly increases the height and width of the absorbance spectrum and LHE, but for the same ratio, Zn material does not change the bandgap of the CZTS absorber material. The sample that produced the best optical properties belonged to the Z125 sample, namely samples fabricated with Zn material with a Zn/Sn ratio of 1.25. The use of Zinc material in a thin layer of CZTS-based solar cell absorber improves performance; namely, there is an increase in V_{oc}, J_{sc} and the efficiency of CZTS-based solar cells. The sample that produced the best performance was owned by the Z125 sample, namely samples fabricated with Zn material with a Zn/Sn ratio of 1.25.

ACKNOWLEDGMENTS

This work was supported by the Penelitian Dasar Unggulan Perguruan Tinggi, Ministry of Education and Culture, Republic of Indonesia 2022.

REFERENCE

[1] Batih, H., Sorapipatana, C., Renewable and Sustainable Energy Reviews. vol **57,** (2016) pp. 1160-1173.
[2] Lestari, N.I., Bulletin of Indonesian Economic Studies. vol **49,** 2 (2013) pp. 239-240.
[3] Lubis, H., Journal of Advanced Research in Applied Sciences and Engineering Technology. vol **11,** 1 (2018) pp. 17-22.
[4] Chelminski, K. Fossil fuel subsidy reform in Indonesia. The politics of fossil fuel subsidies and their reform: Cambridge University Press; (2018). pp. 193-211.
[5] Omer, A.M., J Sust Dev Stud. vol **1,** 1 (2012) pp. 1-67.
[6] Gustafson, A., Marlon, J.R., Goldberg, M.H., Wang, X., Ballew, M.T., Rosenthal, S.A., et al., Environment: Science and Policy for Sustainable Development. vol **62,** 2 (2020) pp. 30-35.
[7] Inglesi-Lotz, R., Dogan, E., Renewable Energy. vol **123,** (2018) pp. 36-43.
[8] Dogan, E., Seker, F., Renewable and Sustainable Energy Reviews. vol **60,** (2016) pp. 1074-1085.
[9] NA, H., International Journal of Renewable Energy Development. vol **1,** 2 (2012) pp. 33-38.
[10] Ho, S.M., Lomi, A., Okoroigwe, E.C., Urrego, L.R., International Journal of Renewable Energy Research. vol **9,** 1 (2019) pp.
[11] Hardianto, H., International Journal of Environment, Engineering & Education. vol **1,** 3 (2019) pp. 1-8.
[12] Santika, W.G., Anisuzzaman, M., Simsek, Y., Bahri, P.A., Shafiullah, G., Urmee, T., Energy. vol **196,** (2020) pp. 117100.
[13] Chapin, D.M., Fuller, C., Pearson, G., Journal of Applied Physics. vol **25,** 5 (1954) pp. 676-677.
[14] Reynolds, D.C., Leies, G., Antes, L.L., Marburger, R.E., Physical Review. vol **96,** 2 (1954) pp. 533-534.
[15] Prima, E.C., Wong, L.H., Ibrahim, A., Yuliarto, B., Optical Materials. vol **114,** (2021) pp. 110947.
[16] Nugroho, H.S., Refantero, G., Prima, E.C., Panatarani, C., Suyatman, Nugraha, N., et al., IOP Conference Series: Materials Science and Engineering. vol **1045,** 1 (2021) pp. 012039.
[17] Refantero, G., Prima, E.C., Setiawan, A., Panatarani, C., Cahyadi, D., Yuliarto, B., Journal of Materials Science: Materials in Electronics. vol **31,** 4 (2020) pp. 3674-3680.
[18] Prawira, Y.Y., Prima, E.C., Refantero, G., Setyo, H., Panatarani, B.Y., International Journal of Nanoelectronics & Materials. vol **13,** 2 (2020) pp. 307-314.
[19] Panatarani, C., Redianti, H., Faizal, F., Cahya Prima, E., Yuliarto, B., Joni, I.M., Key Engineering Materials. vol **860,** (2020) pp. 42-50.
[20] Prima, E.C., Nugroho, H.S., Nugraha, Refantero, G., Panatarani, C., Yuliarto, B., RSC Advances. vol **10,** 60 (2020) pp. 36873-36886.
[21] Prima, E.C., Nuruddin, A., Yuliarto, B., Kawamura, G., Matsuda, A., New Journal of Chemistry. vol **42,** 14 (2018) pp. 11616-11628.
[22] Prima, E.C., Hidayat, N.N., Yuliarto, B., Suyatman, Dipojono, H.K., Spectrochim Acta Mol Biomol Spectrosc vol **171,** (2017) pp. 112-125.
[23] Prima, E.C., Yuliarto, B., Suyatman, Dipojono, H.K., AIP Conf Proc. vol **1677,** (2015) pp. 120002.

[24] Cahya Prima, E., Yuliarto, B., Kresno Dipojono, H., Adv Mat Res vol **1112,** (2015) pp. 317-320.
[25] Prima, E.C., Yuliarto, B., Suendo, V., Suyatman, J Mater Sci Mater Electron vol **25,** 10 (2014) pp. 4603-4611.
[26] Adhyaksa, G.W.P., Prima, E.C., Lee, D.K., Ock, I., Yatman, S., Yuliarto, B., et al., Adv Energy Mater. vol **4,** 18 (2014) pp. 1400470.
[27] Fernández-Werner, L., Faccio, R., Juan, A., Pardo, H., Montenegro, B., Mombrú, Á.W., Applied Surface Science. vol **290,** (2014) pp. 180-187.
[28] Neamen, D.A., "Semiconductor physics and devices: basic principles: New York, NY: McGraw-Hill; (2012) pp.
[29] Katagiri, H., Jimbo, K., Maw, W.S., Oishi, K., Yamazaki, M., Araki, H., et al., Thin Solid Films. vol **517,** 7 (2009) pp. 2455-2460.
[30] Seo, D.-K., Hoffmann, R., Theoretical Chemistry Accounts. vol **102,** 1 (1999) pp. 23-32.
[31] Kato, T., Japanese Journal of Applied Physics. vol **56,** 4S (2017) pp. 04CA02.
[32] Akhavan, V.A., Goodfellow, B.W., Panthani, M.G., Steinhagen, C., Harvey, T.B., Stolle, C.J., et al., Journal of Solid State Chemistry. vol **189,** (2012) pp. 2-12.
[33] Ito, K., Nakazawa, T., Japanese Journal of Applied Physics. vol **27,** 11R (1988) pp. 2094.
[34] Hadke, S.H., Levcenko, S., Lie, S., Hages, C.J., Márquez, J.A., Unold, T., et al., Advanced Energy Materials. vol **8,** 32 (2018) pp. 1802540.
[35] Friedlmeier, T.M., Wieser, N., Walter, T., Dittrich, H., Schock, H. Heterojunctions based on Cu2ZnSnS4 and Cu2ZnSnSe4 thin films. Proceedings of the 14th European Conference of Photovoltaic Science and Engineering and Exhibition1997.
[36] Indonesia, "Undang-Undang No. 4 Tahun 2009 tentang pertambangan mineral dan batubara: Justika Siar Publika; (2009) pp.
[37] Herawati, N., Suzuki, S., Hayashi, K., Rivai, I., Koyama, H., Bulletin of environmental contamination and toxicology. vol **64,** 1 (2000) pp. 33-39.
[38] Wang, W., Winkler, M.T., Gunawan, O., Gokmen, T., Todorov, T.K., Zhu, Y., et al., Advanced Energy Materials. vol **4,** 7 (2014) pp. 1301465.
[39] Liu, W.-S., Chen, S.-Y., Huang, C.-S., Lee, M.-Y., Kuo, H.-C., Journal of Alloys and Compounds. vol **853,** (2021) pp. 157237.
[40] Mendis, B.G., Goodman, M.C., Major, J.D., Taylor, A.A., Durose, K., Halliday, D.P., Journal of Applied Physics. vol **112,** 12 (2012) pp. 124508.
[41] Pal, K., Singh, P., Bhaduri, A., Thapa, K.B., Solar Energy Materials and Solar Cells. vol **196,** (2019) pp. 138-156.
[42] Shin, B., Gunawan, O., Zhu, Y., Bojarczuk, N.A., Chey, S.J., Guha, S., Progress in Photovoltaics: Research and Applications. vol **21,** 1 (2013) pp. 72-76.
[43] Li, W., Tan, J.M.R., Leow, S.W., Lie, S., Magdassi, S., Wong, L.H., Energy Technology. vol **6,** 1 (2018) pp. 46-59.
[44] Huang, T.J., Yin, X., Qi, G., Gong, H., physica status solidi (RRL) – Rapid Research Letters. vol **08,** 09 (2014) pp. 735-762.
[45] Ali, A., Jacob, J., Arshad, M.I., un Nabi, M.A., Ashfaq, A., Mahmood, K., et al., Solid State Sciences. vol**,** (2020) pp. 106198.
[46] Larramona, G., Levcenko, S., Bourdais, S., Jacob, A., Choné, C., Delatouche, B., et al., Advanced Energy Materials. vol **5,** 24 (2015) pp. 1501404.
[47] Guo, Q., Ford, G.M., Yang, W.-C., Walker, B.C., Stach, E.A., Hillhouse, H.W., et al., Journal of the American Chemical Society. vol **132,** 49 (2010) pp. 17384-17386.
[48] Park, J., Huang, J., Yun, J., Liu, F., Ouyang, Z., Sun, H., et al., Advanced Energy Materials. vol **8,** 23 (2018) pp. 1701940.